Investigation of Excitonic Gates in Organic Semiconductor Thin Films

Deepesh Rai and Russell J. Holmes*

Department of Chemical Engineering and Materials Science, University of Minnesota, Minneapolis, Minnesota 55455, USA

(Received 21 June 2018; revised manuscript received 15 November 2018; published 24 January 2019)

We demonstrate that interfaces can play a significant role in overcoming the diffusive and subdiffusive nature of exciton transport in organic semiconductors. By designing interfaces with an imbalance between the forward and reverse rates of energy transfer, the interface can act as a gate, thereby directing exciton transport. While previous work has examined from a theoretical perspective the function of multiple exciton gates arranged in series, we provide a combined theory-experiment treatment that permits an assessment of the utility of exciton-permeable gating interfaces in optoelectronic devices. The required asymmetry in interfacial-exciton-transfer rates is realized by engineering a molecular site imbalance. The impact of interfaces on exciton transport is considered by optically injecting excitons into the gating architecture, and detecting those that migrate through the structure using a luminescent sensitizer. For exciton transport in the archetypical organic fluorescent dye 2,3,6,7-tetrahydro-1,1,7,7,-tetramethyl-1H,5H,11H-10(2-benzothiazolyl) quinolizino-[9,9a,1gh] coumarin (C545T) diluted in the wide-gap organic semiconductor p-bis(triphenylsilyl)benzene (UGH2), a more than 200% improvement in transport efficiency is found in an architecture with properly optimized gates compared to a neat film of C545T.

DOI: 10.1103/PhysRevApplied.11.014048

I. INTRODUCTION

Exciton transport plays a critical role in organic optoelectronic devices, most notably in organic photovoltaic cells (OPVs). In an OPV, photogenerated excitons must diffuse to an electron donor-acceptor heterojunction where exciton dissociation occurs via charge transfer [1–3]. Exciton transport has long been recognized as a key process limiting efficiency in the simplest planar heterojunction cells. Indeed, state-of-the-art OPVs overcome this bottleneck and realize high efficiency through the use of a bulk heterojunction (BHJ) architecture where donor and acceptor materials are blended in a single layer [4–6]. While this approach circumvents the short exciton-diffusion length (L_D) by increasing the area of the dissociating donor-acceptor interface, several works have also attempted to directly increase the value of L_D via molecular design and morphology engineering [7–12]. Indeed, the largest values of L_D have been realized in large-grained polycrystalline thin films and molecular crystals [2,7,9,13–15], though the associated anisotropy means that crystallinity alone does not guarantee long L_D in a given direction [8,16–19]. Prior work has also demonstrated how variations in intermolecular separation can lead to increases in the L_D by optimizing the various parameters responsible for dipole-mediated Förster energy transfer [20–23].

In contrast, less attention has been paid to the more general problem of overcoming the diffusive and subdiffusive nature of exciton transport in organic semiconductors. Menke *et al.* [24] have previously examined the idea of using multiple interfaces with an optimized molecular site imbalance to introduce asymmetry in forward and reverse exciton-transport rates, pushing the system into a regime of anomalous diffusion. Practically, the site imbalance was realized by diluting the active material of interest into a wide energy-gap host by different amounts on either side of the interface [20,23,24]. Indeed, this previous work found a nonlinear dependence of the mean square displacement (MSD) on time (i.e., $\langle x^2 \rangle \propto t^{\alpha}$, $\alpha > 1$), suggesting superdiffusive transport [24]. An imbalance in energy transport rates at an interface can also arise from a difference in energy gap between the two layers. In these architectures, reverse exciton transfer is hindered due to conservation of energy. While not frequently considered in the context of exciton gating, several reports of this type of structure exist in the context of energy cascade devices in which multiple donor or acceptor layers are combined in series to realize high efficiency [25–28]. For structures that rely on a molecular site imbalance, only the case of a single asymmetric interface has been experimentally examined. Here, we offer a combined theoretical-experimental study of the impact of multiple exciton gating interfaces on exciton transport, and hence, a practical assessment of these architectures for devices.

*rholmes@umn.edu

This paper is organized as follows. Section II describes the experimental methods including device fabrication and characterization techniques, while Sec. III describes the models used for data analysis. The results are presented and discussed in Sec. IV, while Sec. V summarizes the conclusions of this work.

II. EXPERIMENT

Exciton transport is examined in multilayer structures where exciton gates are formed by a molecular site imbalance across an interface. Exciton transport is probed in the archetypical fluorescent emitter, 3,6,7-tetrahydro-1,1,7,7, -tetramethyl-1H,5H,11H-10(2-benzothiazolyl) quinolizino -[9,9a,1gh] coumarin (C545T). The interfacial site imbalance is engineered by diluting C545T into a wide energy-gap host material, p-bis(triphenylsilyl)benzene (UGH2) [20,23,29]. In this arrangement, UGH2 is not excited and does not quench excitons from C545T. The architectures of interest are shown in Fig. 1(a), with the associated optical properties of each active material shown in Fig. 1(b). In Fig. 1(a), the gating region of the device containing C545T in various concentrations is sandwiched between an exciton injection layer of N, N′-di-1- naphthalenyl-N,N′-diphenyl [1,1′:4′,1″:4″,1‴-quaterphenyl]-4,4‴-diamine (4P-NPB) [30] and an exciton collecting layer of platinum(II) tetra-phenyl-tetra-benzoporphyrin (PtTPTBP) diluted in UGH2 [31–35]. The PtTPTBP is diluted into a layer of UGH2 in order to increase its photoluminescence (PL) efficiency. The function of this architecture is discussed further in Secs. III and IV. All layers are prepared by thermal vacuum sublimation ($<7\times10^{-7}$ Torr) at a deposition rate of 0.1 nm s^{-1}. All optical constants and thin-film thickness are measured using a J. A. Woollam variable-angle spectroscopic ellipsometer. All of C545T, UGH2, and 4P-NPB are purchased from Luminescence Technology Corporation, while PtTPTBP is purchased from Frontier Scientific. Quartz substrates are sequentially cleaned using tergitol, deionized water, acetone, and isopropanol. Photoluminescence spectra are measured using a Photon Technology International QuantaMaster 400 Fluorometer. Samples are excited at an angle of 70° to sample normal using a monochromatic Xe lamp. All PL measurements are made under a N_2 purge. For PL measurements on exciton gating architectures, the emission scan is carried out in two stages. First, a long pass filter with a cut-off wavelength of $\lambda = 364$ nm is used to prevent pump detection while sample emission is scanned from 370 to 720 nm. Second, sample emission is collected from 600 to 900 nm using a long pass filter with a cut-off wavelength of $\lambda = 600$ nm, to prevent the detection of the 4P-NPB emission double from the sample.

The exciton diffusion length of C545T in UGH2 is measured using thickness-dependent PL quenching

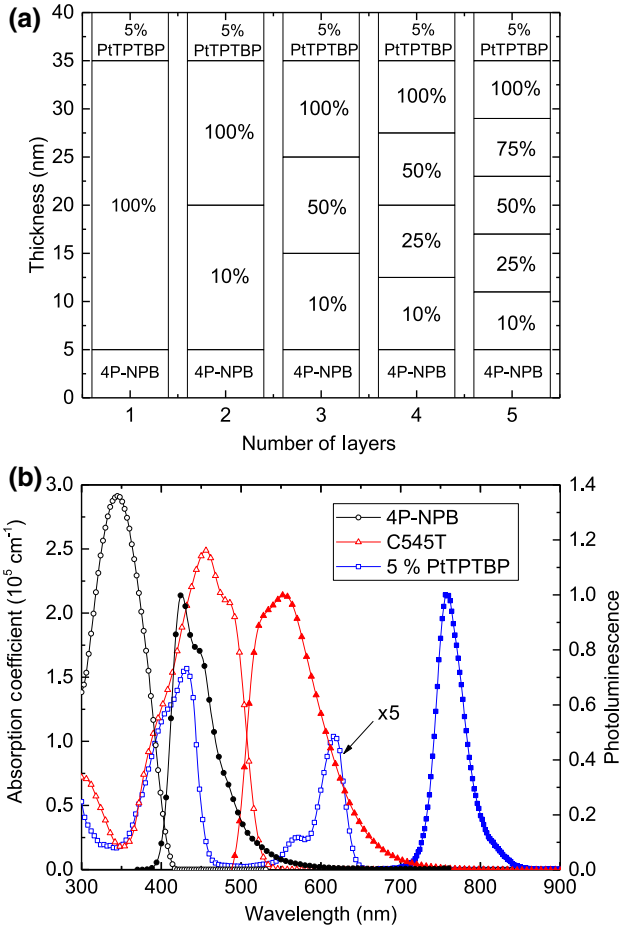

FIG. 1. (a) Layer structure for probing the role of multiple interfacial gates. Excitons are injected from the most dilute layer of C545T in UGH2 (concentration % noted) by energy transfer from an injection layer of 4P-NPB and are collected using a sensitizer layer containing PtTPTBP. The thickness for each layer is optimized to maximize collection. (b) Absorption coefficient (open symbols) and normalized PL (closed symbols) of C545T, 4P-NPB, and 5% PtTPTBP in UGH2. The absorption coefficient is calculated using the extinction coefficient, extracted from ellipsometric measurements on a 30-nm-thick film deposited on glass substrate. Excitons are injected into C545T by pumping 4P-NPB at a wavelength of $\lambda = 355$ nm .

[34]. Thin films of C545T in UGH2 are deposited with and without an adjacent bottom surface quenching layer of 1,4,5,8,9,11-hexaazatriphenylene hexacarbonitrile (HATCN) [21]. Under optical excitation at a wavelength of $\lambda = 460$ nm, the fraction of C545T excitons reaching the quenching interface varies depending on the thickness. A PL ratio is extracted as a function of C545T layer thickness as the ratio of the integrated PL spectrum with and without an adjacent quenching layer. The experimentally obtained PL ratios are modeled using a one-dimensional (1D) steady-state diffusion equation with the exciton diffusion length as the fit parameter. The exciton

generation profile in this model is solved using a transfer matrix formalism [35]. Photoluminescence efficiencies are measured using an integrating sphere with previously published methods [36]. Exciton lifetimes are measured using a PicoQuant time-correlated single-photon-counting (TCSPC) system, excited at a wavelength of $\lambda = 470$ nm using 70-ps laser pulses.

III. THEORY

Exciton diffusion in organic semiconductor thin films can be treated as an ensemble of intermolecular hopping events. The rate of excitonic energy transfer k_{ET} can be related to the exciton diffusivity (D) and diffusion length (L_D) for transport in a simple cubic lattice as

$$D = \frac{1}{6}\sum\nolimits_N d^2 k_{\mathrm{ET}}(d) = \frac{L_D^2}{\tau}, \tag{1}$$

where d is the intermolecular spacing assuming a cubic lattice, τ is the exciton lifetime, and N is the number of molecular hopping sites [2,13,37]. In spin-singlet fluorescent materials, the dominant mechanism for energy transfer is usually considered to be a point-to-point, dipole-mediated, nonradiative Förster transfer [1–3,38], with the rate given as

$$k_F(d) = \frac{1}{\tau}\left(\frac{R_0}{d}\right)^6, \tag{2}$$

where R_0 is the Förster radius, τ is the exciton lifetime, and d is the distance between donor and acceptor molecules. The Förster radius (R_0) is separately defined as [1–3,38]

$$R_0^6 = \frac{9\eta_{PL}\kappa^2}{128\pi^5}\int \frac{\lambda^4 F_D(\lambda)\sigma_A(\lambda)d\lambda}{n(\lambda)^4}, \tag{3}$$

where η_{PL} is the photoluminescence efficiency, κ is the dipole orientation factor (taken as $0.845\sqrt{2/3}$ for randomly oriented rigid dipoles) [2,39], n is the wavelength-dependent refractive index of the donor film, F_D is the normalized fluorescence spectrum, σ_A is the acceptor absorption cross section, and λ is the wavelength. For an isotropic film, there is an equal probability of the exciton hopping in all directions. In a 1D analog, this implies transport in the forward and reverse directions is equally likely. When the exciton encounters an asymmetric interface with differing forward and reverse rates of energy transfer, a more detailed analysis is required.

Here, we consider the case of an interface across which there is a difference in the density of molecular sites and intermolecular spacing for a single material species (Fig. 2). In order to treat energy transfer from a molecule on one side of the interface to a plane of molecules on the other side of the interface, we consider a rate that varies

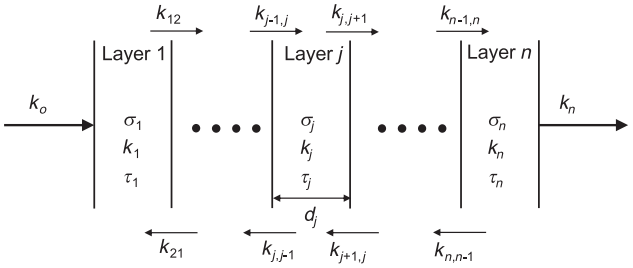

FIG. 2. A general multilayer structure having n layers between the injection layer and sensitizer layer. Each layer j ($j = 1, 2, 3, \ldots, n$) has a thickness d_j, areal density σ_j of donor molecules in a wide-gap host material, a bulk energy transfer rate k_j, and an exciton lifetime τ_j. The energy transfer rate between the plane of molecules in layers i and j is represented by k_{ij}.

with the intermolecular separation (d) as d^{-4} and is directly proportional to the areal density of acceptor molecules [40–42]. Thus, the energy transfer rate across the interface is given as

$$k_{ij} = k_i \times \frac{\sigma_j}{\sigma_i} \times \frac{d_i^4}{d_{ij}^4} \times \frac{R_{ij}^6}{R_i^6}, \tag{4}$$

where k_i and k_j are the respective bulk rates of Förster energy transfer in layers i and j, σ_i and σ_j are the areal densities of molecules in layer i and layer j, and R_{ij} and R_{ji} are the Förster radii for forward and reverse transfer across the interface. In considering energy transfer across an interface, it is assumed that the degree of excitonic-energetic disorder does not change with dilution [18,43,44]. Were it to change substantially, disorder could add an additional source of asymmetry across the interface for the rates of energy transfer. With Eq. (4), a Kinetic Monte Carlo (KMC) formalism is used to examine the effect of interfacial rate asymmetry on the exciton transport efficiency (η_T) across a gating architecture. The KMC simulation solves the exciton-diffusion equation without prior information regarding interfacial boundary conditions by using the known imbalance in energy transfer rates [24,45,46]. This approach divides each layer of the architecture into bins that are 1-nm thick. Each bin is assigned a set of local generation, energy transfer, and natural decay rates for the various events that govern exciton behavior during its lifetime. Generation rates are calculated using an optical transfer matrix formalism that takes as inputs layer thicknesses and optical constants, both determined via ellipsometry [35]. Energy transfer rates are extracted from the experimental value of L_D as described in Sec. IV. The natural decay rate of the exciton is measured using transient fluorescence as described in Sec. II. We note that the KMC approach used here differs slightly from that of Ref. [24] in that long-range energy transfer between nonadjacent layers is explicitly included in the calculations.

The KMC formalism was first verified against an analytical model for exciton diffusion in a single layer with an adjacent quencher (See Supplemental Material [47], Fig. S3).

IV. RESULTS AND DISCUSSION

In the architectures of Fig. 1(a), the relative role of the gates on exciton transport is considered in terms of η_T. Excitons are injected from 4P-NPB into C545T by optically pumping at a wavelength of $\lambda = 355$ nm, where absorption occurs mainly in the 4P-NPB layer [30]. The exciton transport efficiency is proportional to the ratio of excitons collected by PtTPTBP to the number of excitons injected from 4P-NPB. Experimentally, η_T is calculated as the ratio of photoluminescence from PtTPTBP and 4P-NPB, while correcting for the differences in PL efficiency and optical-outcoupling efficiency. These calculations are discussed further in the Supplemental Material [47], are fully determined from experimental data, and do not introduce any free parameters into the analysis.

For the architectures of Fig. 1(a), the overall thickness of the gating region is fixed at 30 nm. Layer concentrations are selected to maximize η_T for the overall structure. For a given series of exciton gates, the transport efficiency is calculated by injecting excitons from the most dilute layer and collecting them from the neat layer of the structure. The simulation of η_T depends on the bulk energy transfer rate (k_i) and the transfer rate between layers (k_{ij}). The k_i in each layer is extracted using Eq. (1) and the experimentally measured value of L_D [Fig. 3(a)] [34,42]. The extracted bulk L_D of C545T decreases with dilution in UGH2 due to increasing molecular separation. This decrease occurs despite an increase in R_0 with dilution. In contrast, the L_D of molecules such as boron subphthalocyanine chloride (SubPc) and boron subnaphthalocyanine chloride (SubNc) have been shown to increase upon dilution in UGH2 due to the prevalence of an increase in R_0 over the increase in molecular separation [20,23].

The rate of energy transfer between layers (k_{ij}) is computed by considering differences in concentration, interbin distance, and R_0 [Eq. (4)]. The R_0 between layers is computed from Eq. (3) using experimentally measured parameters such as the PL efficiency, refractive index of the donor medium, and spectral overlap integral, while the orientation factor is taken for randomly oriented dipoles [39]. Denoting layers i and j in Fig. 2 as the donor and acceptor, respectively, Fig. 3(b) plots the Förster radius for energy transfer (R_0) from layer i to layer j as a function of acceptor concentration for different donor concentrations of C545T in UGH2. For a fixed acceptor concentration, an increase in R_0 is observed with a reduced concentration of the donor C545T in UGH2. This observation reflects a concomitant increase in the PL efficiency from $(9 \pm 1)\%$ in neat film to $(37 \pm 2)\%$ for 10 wt. % C545T in UGH2, as well as an increase in the spectral overlap integral due to a blue shift in the fluorescence with dilution. The index of refraction also decreases with dilution from a value of 2.5 in neat film to a value of 1.7 for 10 wt. % C545T in UGH2. At a fixed donor concentration, the increase in R_0 with acceptor concentration reflects an increase in the spectral overlap integral, driven by an increase in the absorption cross section of the acceptor layer of C545T in UGH2.

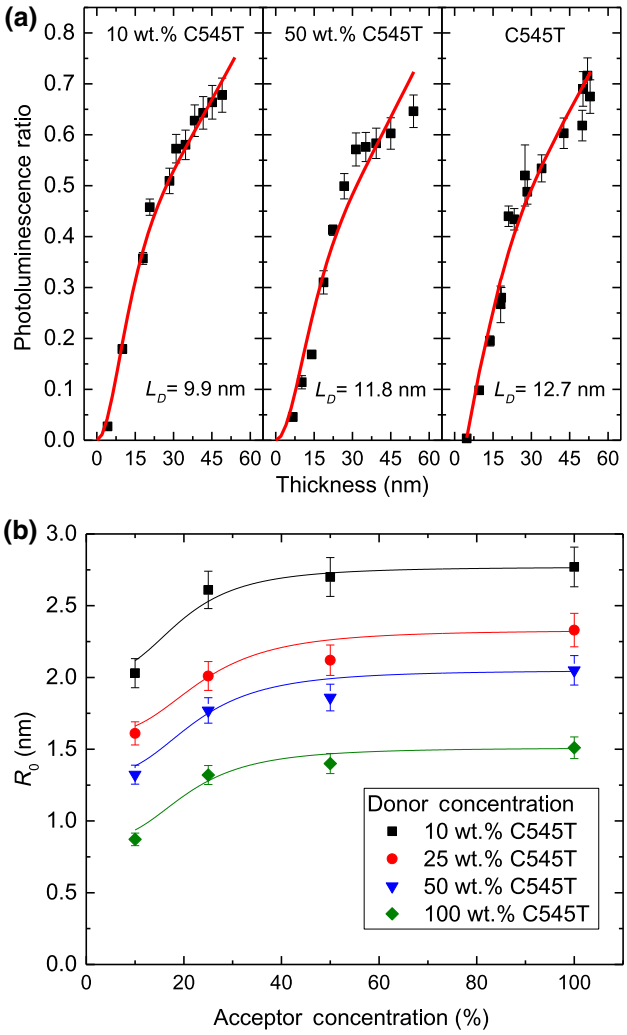

FIG. 3. (a) Photoluminescence ratio versus thickness for three different concentrations of C545T diluted in UGH2. The L_D is extracted by fitting experimental data using a 1D steady-state diffusion equation. (b) Förster radius (R_0) as a function of acceptor layer concentration for different C545T donor layer concentrations in UGH2. The solid lines are guides for the eye.

The PL intensity of PtTPTBP is tracked as a proxy for η_T as the number of layers is varied [Fig. 4(a)]. Varying the number of layers changes the number of locations where the exciton experiences asymmetry in energy transfer rates, and the degree of gating and directed exciton transport. Interestingly, η_T [Fig. 4(b)] is maximized when the number of layers is ≥ 3. This plateau is reproduced

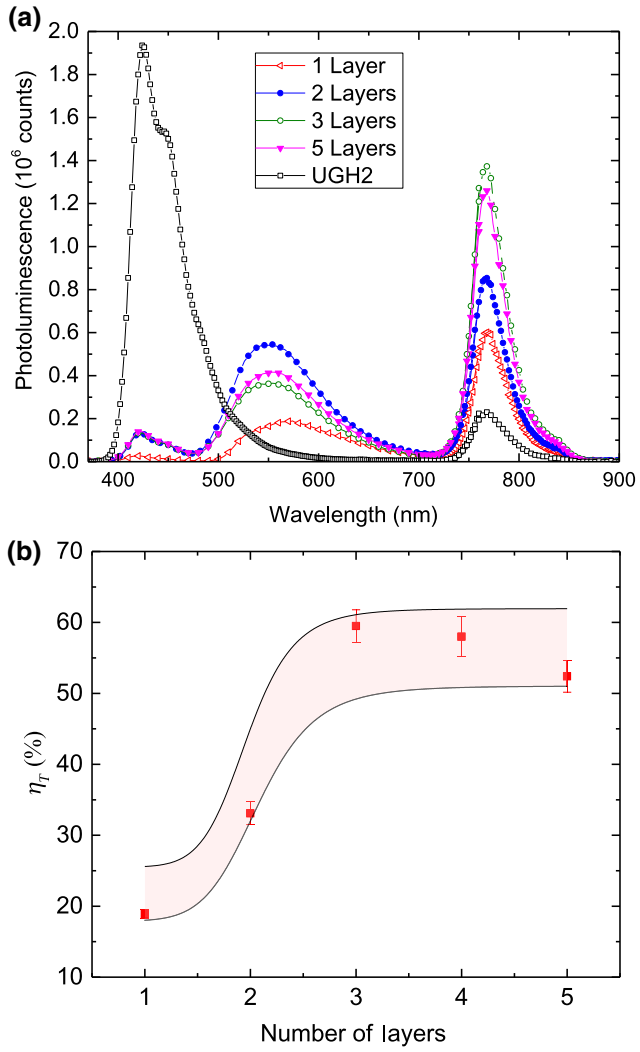

FIG. 4. (a) Photoluminescence spectrum of the structures in Fig. 1(a) pumped at a wavelength of $\lambda = 355$ nm. (b) Experimental and simulated (lines) transport efficiency as a function of the number of layers. The two lines indicate the upper and lower bounds of the simulated structure accounting for error in the measured L_D and layer thickness.

well by the associated KMC simulation shown in Fig. 4(b) as a pair of solid lines. The two lines are the upper and lower bounds of η_T for the simulated structure accounting for error in the measured L_D of C545T and the layer thicknesses. The good agreement between the simulation and experiment confirms that the model has accurately captured the physics of gating interfaces. An important feature of the KMC simulation used here is the inclusion of long-range energy transfer between nonadjacent bins in the calculations. Energy transfer between nonadjacent layers contributes 3% and 9% of the total transport efficiency for the 3-layer and 5-layer structures, respectively. This contribution will increase as the distance between nonadjacent layers approaches R_0.

In considering the impact of the results of Fig. 4(b) on device design, it is important to consider the origin of the observed plateau in η_T. The plateau is intrinsic to the use of concentration to establish the gates, reflecting a trade-off between the number of interfaces and the strength of an individual gate to drive asymmetric exciton transport. While this plateau would not occur in energy off-set driven gates found in cascade OPVs [23–25], such structures inherently come with an undesirable relaxation of the exciton as it migrates. In this work, the use of concentration-driven exciton gates leads to a $>200\%$ increase in η_T compared to a neat film of C545T with no gates [Fig. 4(b)]. This is equivalent to an effective increase in L_D from 12.7 to approximately 35 nm, further demonstrating the potential gains to be realized by engineering interfaces for enhanced exciton harvesting.

V. CONCLUSIONS

In conclusion, interfacial excitonic gates are experimentally created through a molecular site imbalance via dilution in a wide-energy-gap material. The effectiveness of these gates is demonstrated by injecting excitons from the most dilute layer and measuring the excitons collected from the neat layer. Experimentally, C545T is used as a testbed to experimentally examine the role of interfacial excitonic gates in tailoring exciton diffusion in an organic semiconductor. It is shown that the incorporation of interfaces introduces asymmetry in exciton motion, thereby improving η_T. However, the competition between the number of interfaces and the strength of an individual gate to drive asymmetric exciton transport leads to a saturation in η_T. The approach of using interfacial gates to enhance exciton transport offers new opportunities in the design of organic optoelectronic devices, and especially planar heterojunction OPVs for improved exciton harvesting.

ACKNOWLEDGMENTS

This work was supported by National Science Foundation (NSF) Electronics, Photonics and Magnetic Devices under Grant No. ECCS-1509121.

[1] O. V. Mikhnenko, P. W. M. Blom, and T.-Q. Nguyen, Exciton diffusion in organic semiconductors, Energy Environ. Sci. **8**, 1867 (2015).
[2] S. M. Menke and R. J. Holmes, Exciton diffusion in organic photovoltaic cells, Energy Environ. Sci. **7**, 499 (2014).
[3] G. J. Hedley, A. Ruseckas, and I. D. W. Samuel, Light harvesting for organic photovoltaics, Chem. Rev. **117**, 796 (2017).
[4] X. Che, Y. Li, Y. Qu, and S. R. Forrest, High fabrication yield organic tandem photovoltaics combining vacuum- and solution-processed subcells with 15% efficiency, Nat. Energy **3**, 422 (2018).

[5] S. Zhang, Y. Qin, J. Zhu, and J. Hou, Over 14% efficiency in polymer solar cells enabled by a chlorinated polymer donor, Adv. Mater. **30**, 1800868 (2018).
[6] L. Meng, Y. Zhang, X. Wan, C. Li, X. Zhang, Y. Wang, X. Ke, Z. Xiao, L. Ding, R. Xia, H. L. Yip, Y. Cao, and Y. Chen, Organic and solution-processed tandem solar cells with 17.3% efficiency, Science **361**, 1094 (2018).
[7] R. R. Lunt, J. B. Benziger, and S. R. Forrest, Relationship between crystalline order and exciton diffusion length in molecular organic semiconductors, Adv. Mater. **22**, 1233 (2010).
[8] S. Rim, R. F. Fink, J. C. Schöneboom, P. Erk, and P. Peumans, Effect of molecular packing on the exciton diffusion length in organic solar cells, Appl. Phys. Lett. **91**, 173504 (2007).
[9] H. Najafov, B. Lee, Q. Zhou, L. C. Feldman, and V. Podzorov, Observation of long-range exciton diffusion in highly ordered organic semiconductors, Nat. Mater. **9**, 938 (2010).
[10] P. M. Beaujuge and J. M. J. Frechet, Molecular design and ordering effects in π-functional materials for transistor and solar cell applications, J. Am. Chem. Soc. **133**, 20009 (2011).
[11] Y. Huang, E. J. Kramer, A. J. Heeger, and G. C. Bazan, Bulk heterojunction solar cells: Morphology and performance relationships, Chem. Rev. **114**, 7006 (2014).
[12] N. Gasparini, A. Wadsworth, M. Moser, D. Baran, I. McCulloh, and C. J. Brabec, The physics of small molecule acceptors for efficient and stable bulk heterojunction solar cells, Adv. Energy Mater. **8**, 1703298 (2018).
[13] R. C. Powell and Z. G. Soos, Singlet exciton energy transfer in organic solids, J. Lumin. **11**, 1 (1975).
[14] D. Kurrle and J. Pflaum, Exciton diffusion length in the organic semiconductor diindenoperylene, Appl. Phys. Lett. **92**, 133306 (2008).
[15] X. H. Jin, M. B. Price, J. R. Finnegan, C. E. Boott, J. M. Richter, A. Rao, S. M. Menke, R. H. Friend, G. R. Whittell, and I. Manners, Long-range exciton transport in conjugated polymer nanofibers prepared by seeded growth, Science **360**, 897 (2018).
[16] G. Wei, R. R. Lunt, K. Sun, S. Wang, M. E. Thompson, and S. R. Forrest, Efficient, ordered bulk heterojunction nanocrystalline solar cells by annealing of ultrathin squaraine thin films, Nano Lett. **10**, 3555 (2010).
[17] H. Y. Shin, J. H. Woo, M. J. Gwon, M. Barthelemy, M. Vomir, T. Muto, K. Takaishi, M. Uchiyama, D. Hashizume, T. Aoyama, D. W. Kim, S. Yoon, J. Bigot, J. W. Wu, and J. C. Ribierre, Exciton diffusion in near-infrared absorbing solution-processed organic thin films, Phys. Chem. Chem. Phys. **15**, 2867 (2013).
[18] O. V. Mikhnenko, J. Lin, Y. Shu, J. E. Anthony, P. W. M. Blom, T. Q. Nguyen, and M. A. Loi, Effect of thermal annealing on exciton diffusion in a diketopyrrolopyrrole derivative, Phys. Chem. Chem. Phys. **14**, 14196 (2012).
[19] B. P. Rand, D. Cheyns, K. Vasseur, N. C. Giebink, S. Mothy, Y. Yi, V. Coropceanu, D. Beljonne, J. Cornil, J. L. Brédas, and J. Genoe, The impact of molecular orientation on the photovoltaic properties of a phthalocyanine/fullerene heterojunction, Adv. Funct. Mater. **22**, 2987 (2012).
[20] S. M. Menke, W. A. Luhman, and R. J. Holmes, Tailored exciton diffusion in organic photovoltaic cells for enhanced power conversion efficiency, Nat. Mater. **12**, 152 (2013).
[21] I. J. Curtin, D. W. Blaylock, and R. J. Holmes, Role of impurities in determining the exciton diffusion length in organic semiconductors, Appl. Phys. Lett. **108**, 163301 (2016).
[22] T. K. Mullenbach, K. A. McGarry, W. A. Luhman, C. J. Douglas, and R. J. Holmes, Connecting molecular structure and exciton diffusion length in rubrene derivatives, Adv. Mater. **25**, 3689 (2013).
[23] S. M. Menke and R. J. Holmes, Energy-cascade organic photovoltaic devices incorporating a host–guest architecture, ACS Appl. Mater. Interfaces **7**, 2912 (2015).
[24] S. M. Menke, T. K. Mullenbach, and R. J. Holmes, Directing energy transport in organic photovoltaic cells using interfacial exciton gates, ACS Nano **9**, 4543 (2015).
[25] K. Cnops, B. P. Rand, D. Cheyns, B. Verreet, M. A. Empl, and P. Heremans, 8.4% efficient fullerene-free organic solar cells exploiting long-range exciton energy transfer, Nat. Commun. **5**, 3406 (2014).
[26] C. W. Schlenker, V. Barlier, S. W. Chin, M. T. Whited, R. E. McAnally, S. R. Forrest, and M. E. Thompson, Cascade organic solar cells, Chem. Mater. **23**, 4132 (2011).
[27] A. Barito, M. E. Sykes, B. Huang, D. Bilby, B. Frieberg, J. Kim, P. F. Green, and M. Shtein, Universal design principles for cascade heterojunction solar cells with high fill factors and internal quantum efficiencies approaching 100%, Adv. Energy Mater. **4**, 1400216 (2014).
[28] V. C. Nikolis, J. Benduhn, F. Holzmueller, F. Piersimoni, M. Lau, O. Zeika, D. Neher, C. Koerner, D. Spoltore, and K. Vandewal, Reducing voltage losses in cascade organic solar cells while maintaining high external quantum efficiencies, Adv. Energy Mater. **7**, 1700855 (2017).
[29] R. J. Holmes, B. W. D'Andrade, S. R. Forrest, X. Ren, J. Li, and M. E. Thompson, Efficient, deep-blue organic electrophosphorescence by guest charge trapping, Appl. Phys. Lett. **83**, 3818 (2003).
[30] G. Schwartz, M. Pfeiffer, S. Reineke, K. Walzer, and K. Leo, Harvesting triplet excitons from fluorescent blue emitters in white organic light-emitting diodes, Adv. Mater. **19**, 3672 (2007).
[31] Y. Sun, C. Borek, K. Hanson, P. Djurovich, M. Thompson, J. Brooks, J. Brown, and S. Forrest, Photophysics of Pt-porphyrin electrophosphorescent devices emitting in the near infrared, Appl. Phys. Lett. **90**, 213503 (2007).
[32] K. W. Hershey, J. Suddard-Bangsund, G. Qian, and R. J. Holmes, Decoupling degradation in exciton formation and recombination during lifetime testing of organic light-emitting devices, Appl. Phys. Lett. **111**, 113301 (2017).
[33] N. C. Erickson and R. J. Holmes, Investigating the role of emissive layer architecture on the exciton recombination zone in organic light-emitting devices, Adv. Funct. Mater. **23**, 5190 (2013).
[34] P. Peumans, A. Yakimov, and S. R. Forrest, Small molecular weight organic thin-film photodetectors and solar cells, J. Appl. Phys. **93**, 3693 (2003).
[35] L. A. A. Pettersson, L. S. Roman, and O. Inganas, Modeling photocurrent action spectra of photovoltaic devices based on organic thin films, J. Appl. Phys. **86**, 487 (1999).

[36] K. Yuichiro, S. Hiroyuki, and A. Chihaya, Simple accurate system for measuring absolute photoluminescence quantum efficiency in organic solid-state thin films, J. Appl. Phys. **43**, 7729 (2004).

[37] R. R. Lunt, N. C. Giebink, A. A. Belak, J. B. Benziger, and S. R. Forrest, Exciton diffusion lengths of organic semiconductor thin films measured by spectrally resolved photoluminescence quenching, J. Appl. Phys. **105**, 053711 (2009).

[38] T. Förster, 10th Spiers Memorial Lecture. Transfer mechanisms of electronic excitation, Discuss. Faraday Soc. **27**, 7 (1959).

[39] R. E. Dale, J. Eisinger, and W. E. Blumberg, The orientational freedom of molecular probes. The orientation factor in intramolecular energy transfer, Biophys. J. **26**, 161 (1979).

[40] D. R. Haynes, A. Tokmakoff, and S. M. George, Distance dependence of electronic energy transfer between donor and acceptor adlayers: p-terphenyl and 9,10-diphenylanthracene, J. Chem. Phys. **100**, 1968 (1994).

[41] S. R. Scully, P. B. Armstrong, C. Edder, J. M. J. Fréchet, and M. D. McGehee, Long-range resonant energy transfer for enhanced exciton harvesting for organic solar cells, Adv. Mater. **19**, 2961 (2007).

[42] S. R. Scully and M. D. McGehee, Effects of optical interference and energy transfer on exciton diffusion length measurements in organic semiconductors, J. Appl. Phys. **100**, 034907 (2006).

[43] S. Athanasopoulos, E. V. Emelianova, A. B. Walker, and D. Beljonne, Exciton diffusion in energetically disordered organic materials, Phys. Rev. B **80**, 195209 (2009).

[44] S. M. Menke and R. J. Holmes, Evaluating the role of energetic disorder and thermal activation in exciton transport, J. Mater. Chem. C **4**, 3437 (2016).

[45] O. G. Reid and G. Rumbles, Resonance energy transfer enables efficient planar heterojunction organic solar cells, J. Phys. Chem. C **120**, 87 (2016).

[46] J. A. Bjorgaard and M. E. Köse, Simulations of singlet exciton diffusion in organic semiconductors: a review, RSC Adv. **5**, 8432 (2015).

[47] See Supplemental Material at http://link.aps.org/supplemental/10.1103/PhysRevApplied.11.014048 for outcoupled photoluminescence efficiency ratio measurement and kinetic Monte Carlo simulation of exciton diffusion.